Journal of ELECTRONIC MATERIALS, Vol. 44, No. 8, 2015
DOI: 10.1007/s11664-015-3720-x

Magnetic and Microwave Properties of Barium Hexaferrite Ceramics Doped with Gd and Nd

MAJID JAMALIAN,[1,2] ALI GHASEMI,[1]
and MOHAMMAD JAVAD POURHOSSEINI ASL[1]

1.—Department of Materials Engineering, Malek Ashtar University of Technology, Isfahan, Iran.
2.—e-mail: mjscience@yahoo.com

Substituted barium hexaferrite nanoparticles with the chemical formula $BaFe_{12-x}(GdNd)_{x/2}O_{19}$ (x = 0–2, in steps of 0.5) were prepared by a co-precipitation method. Phase identification and crystal structure of the nanoparticles were investigated by x-ray diffraction. The morphology of the nanopowders was investigated by field-emission scanning electron microscopy. Results from Fourier-transform infrared spectroscopy enabled identification of stretching and bending modes. Magnetic properties were measured by use of a vibrating sample magnetometer. The results revealed that saturation magnetization and coercivity decreased as x increased. Investigation of microwave-absorption properties, by use of a vector network analyzer, revealed that the maximum reflection loss of substituted Ba-ferrite of thickness 1.6 mm reached −41.8 dB at a frequency of 4.3 GHz and a bandwidth of 7.5 GHz, with reflection loss being >-20 dB. From these results it was concluded that the composites had good potential as absorbers in the gigahertz frequency range.

Key words: Barium ferrite, magnetic properties, microwave absorption

INTRODUCTION

Barium ferrite ($BaFe_{12}O_{19}$) is used in the electronics industry because it is inexpensive and has high coercivity, chemical stability, anisotropy, and corrosion resistance.[1–4] M-type barium hexaferrites have a magnetoplumbite structure[5] and their magnetic properties are inherently related to their crystalline nature. They all have magneto-crystalline anisotropy; that is, induced magnetization has a predominant orientation inside the crystalline structure.[6–9] Technological applications of BaM require not only fine particle size, with a narrow size distribution, but also a chemically homogeneous microscopic structure.[10] Several procedures, including chemical and mechanical methods, have been used to prepare barium ferrite particles. Because they result in a homogenous product with a narrow particle size distribution, chemical methods are regarded as superior to mechanical methods.

(Received September 8, 2014; accepted February 25, 2015; published online March 13, 2015)

This paper deals with the production of very-high-coercivity barium hexaferrite ceramic nanoparticles by a co-precipitation method. To study the effect of doping of ferrites by other particles in improving both the magnetic and microwave properties of the composite, and to obtain desired nanoparticles, Gd and Nd were added before chemical syntheses.

EXPERIMENTAL

Samples were prepared by a co-precipitation method, with barium chloride dehydrate ($BaCl_2{\cdot}2H_2O$, 99%; Merck, Germany), iron(III) chloride ($FeCl_3$, 99%; Merck), gadolinium chloride ($GdCl_3$, 99%; Merck), neodymium chloride ($NdCl_3$, 99%; Merck), and sodium hydroxide (NaOH, 99%; Merck) as starting materials. Stoichiometric amounts of the metal salts were weighed and mixed with distilled water for 30 min; NaOH solution (1 M), as precipitating agent, was then added dropwise to the mixture to adjust the solution pH to 13. The solution containing the precipitate was then stirred for 2 h. The precipitates were washed five times with water to reduce the pH to 7; then dried at 100°C in an oven

and calcined at 900°C in a programmed furnace for 1 h at a heating rate of 10°C/min.

The crystal structure was investigated, at ambient temperature, by use of a Philips MPD-X'pert HighScore x-ray diffraction (XRD) instrument with Cuk_{α} radiation. The morphology of the nanoparticles was investigated by field-emission scanning electron microscopy (FESEM; Tescan-Mira II). A Fourier-transform infrared spectrometer (FTIR, ISCO-680PLUS) was used to examine formation of the BaM hexaferrites. The magnetic properties and microwave characteristics were studied by use of a vibrating sample magnetometer (VSM, TM-XYZTB-SIH) and a vector network analyzer (VNA, HP 8722ET), respectively.

RESULTS AND DISCUSSION

Structural and Morphological Evaluation

Figure 1 shows the XRD patterns of $BaFe_{12-x}(GdNd)_{x/2}O_{19}$ (x = 0–2) nanoparticles. The XRD patterns contain impurity lines, possibly Fe_2O_3, from x = 0 to x = 2. The reason for formation of the impurity was the low annealing temperature. The peaks of the doped barium ferrites were not at the same precise positions as those of the undoped ferrite; their intensities were also different. The shift in the position of the peaks was because of substitution of Fe^{3+} (0.645 Å) with Gd^{3+} (0.935 Å) and Nd^{3+} (0.983 Å) cations of different ionic radius. The diffraction peaks at 2θ = 30.42°, 32.24°, 34.20°, 35.71°, 37.18°, 40.41°, 55.09°, 56.63°, and 63.11° arose from the (110), (107), (114), (108), (203), (205), (217), (304), and (220) planes, in accordance with JCPDS: 00-007-0276 and 01-074-1121. Cell constants (a, c, and c/a) and cell volume (V) are calculated by use of appropriate formulae:

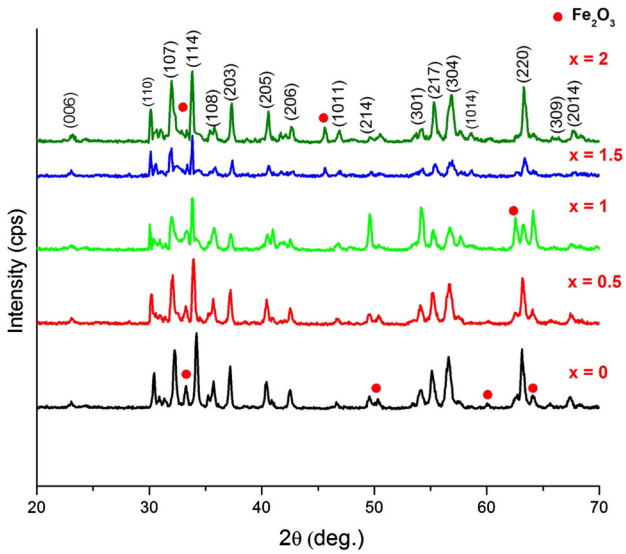

Fig. 1. X-ray diffraction patterns of $BaFe_{12-x}(GdNd)_{x/2}O_{19}$.

$$\frac{1}{d^2} = \frac{4}{3}\left(\frac{h^2 + hk + k^2}{a^2}\right) + \frac{l^2}{c^2} \quad (1)$$

$$V = 0.8666a^2c \quad (2)$$

where d is the distance between two crystallographic planes (hkl) and a and c are the unit cell constants.[11] First, it is necessary to choose two appropriate peaks (107, 114) which are dominant throughout the pattern. a and c can then be calculated by use of Eq. 1. Equation 2 was used to calculate the volume of the unit cell (V).

Table I shows the lattice constants for these samples. The behavior of the lattice constants a and c differed for these samples; basically, a gradually increased with increasing Gd–Nd concentration up to the stoichiometric amount of x = 2 (5.989 Å). The reason for the increase could be occupation of more Fe^{3+} (0.645 Å) sites by Gd^{3+} and Nd^{3+} with larger ionic radii (0.935 and 0.983 Å, irrespectively), resulting in a shift in the peaks of XRD patterns toward lower angles.

FESEM images of $BaFe_{12-x}(GdNd)_{x/2}O_{19}$($x$ = 0–2) calcined at 900°C are shown in Fig. 2. All micrographs contain both BaM and Fe_2O_3, with the percentage of barium hexaferrite increasing with increasing substitution whereas the percentage of Fe_2O_3 decreases. For instance, the sample for which x = 0 contains 87.43% $BaFe_{12}O_{19}$ and 12.57% Fe_2O_3, whereas the sample for which x = 2 contains 89.07% $BaFe_{10}GdNdO_{19}$ and 10.93% Fe_2O_3. The FESEM images reveal the morphology and shape of nanoparticles. It was discovered that addition of Gd–Nd affected the particles sizes of $BaFe_{12-x}(GdNd)_{x/2}O_{19}$($x$ = 0–2). Because Gd–Nd substitution might reduce the crystallization temperature, crystalline ferrite may be formed at lower temperatures, consequently providing more growth time for

Table I. Lattice constants for $BaFe_{12-x}(GdNd)_{x/2}O_{19}$ (x = 0–2)

$BaFe_{12-x}(GdNd)_{x/2}O_{19}$	a (Å) ± 0.01	c (Å) ± 0.01	c/a ± 0.01	V (Å^3) ± 0.01
x = 0	5.878	23.130	3.935	692.554
x = 0.5	5.909	23.250	3.935	703.509
x = 1	5.943	23.263	3.914	712.026
x = 1.5	5.977	23.265	3.892	720.258
x = 2	5.989	23.267	3.885	723.215

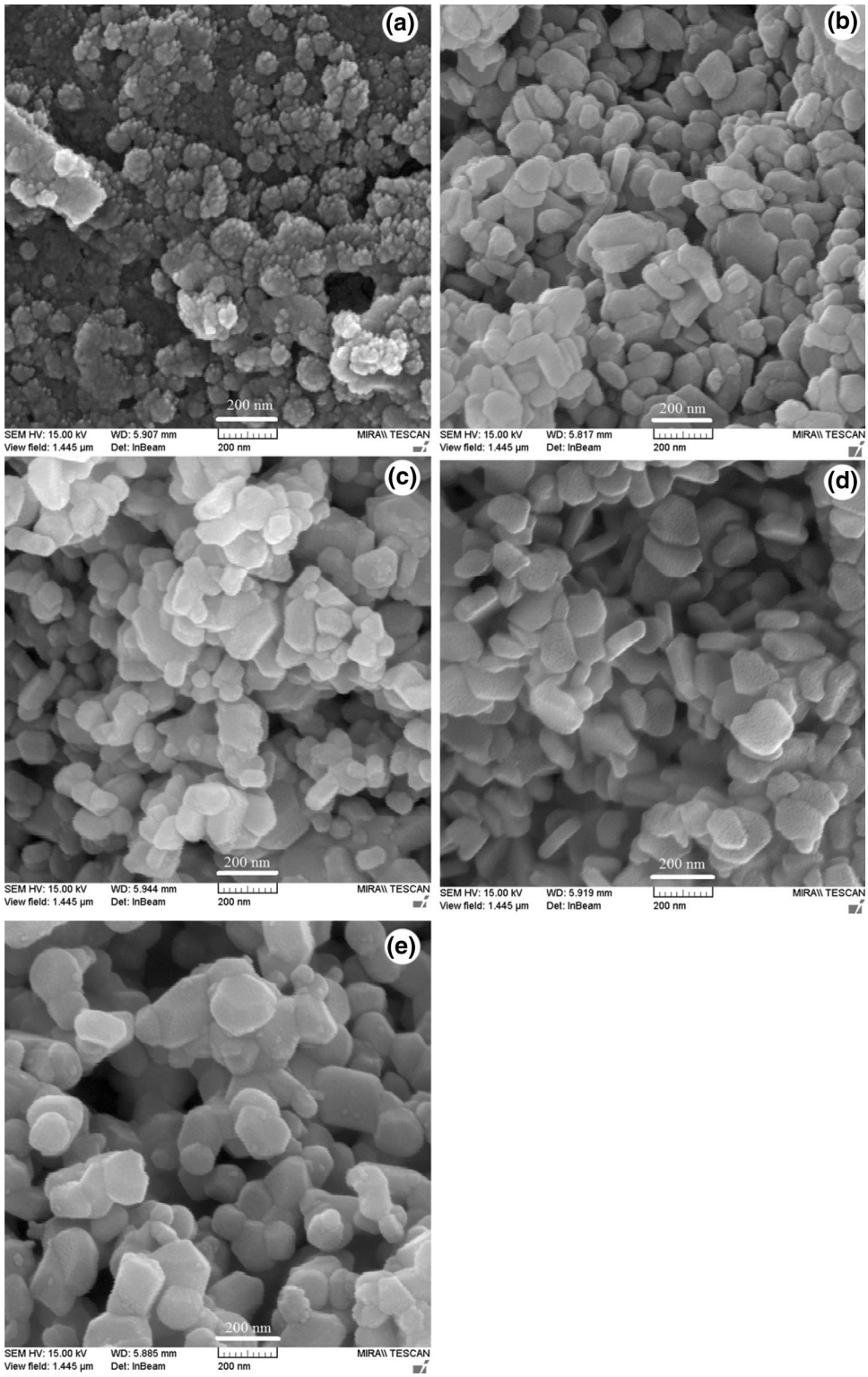

Fig. 2. Field emission scanning electron micrographs of $BaFe_{12-x}(GdNd)_{x/2}O_{19}$ with x = (a) 0 (b) 0.5 (c) 1 (d) 1.5 (e) 2.

nanoparticles up to 900°C. Moreover, small nanoparticles are prone to melt at a lower temperatures than large nanoparticles, as a result of the vigorous driving forces of their high surface energies, owing to their large specific surface areas. Therefore, an increase in particle size occurred with increasing dopant content. An image analyzer was used to calculate the mean particle size of the

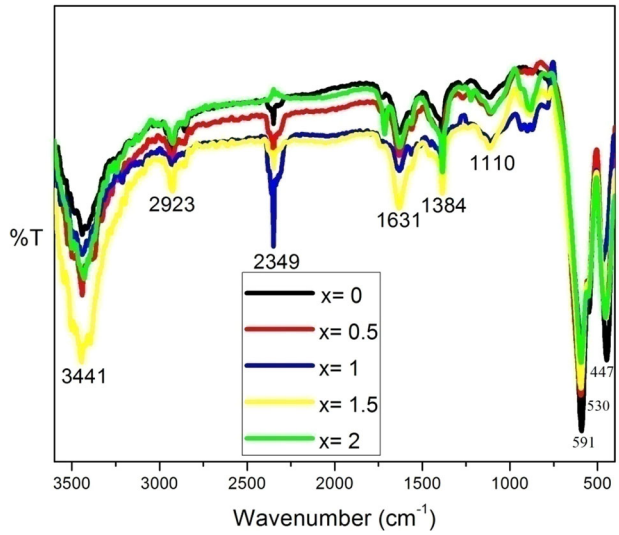

Fig. 3. FTIR spectra of $BaFe_{12-x}(GdNd)_{x/2}O_{19}$.

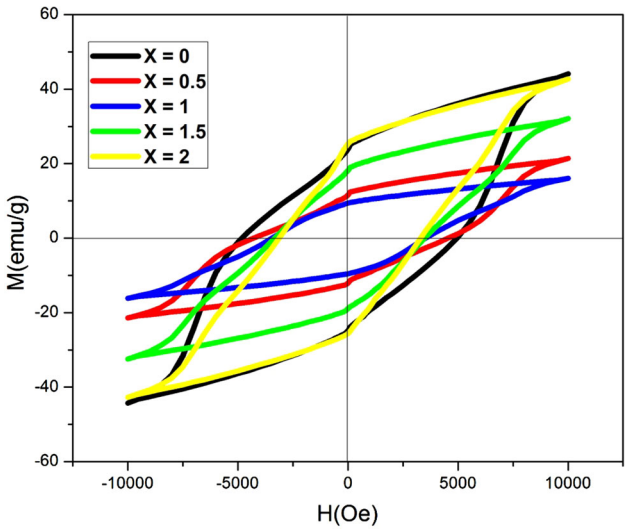

Fig. 4. Magnetic hysteresis of $BaFe_{12-x}(GdNd)_{x/2}O_{19}$.

samples. The mean particle sizes of samples with x = 0, 0.5, 1, 1.5 and 2 were 46 ± 2, 68 ± 2, 73 ± 2, 81 ± 2, and 95 ± 2 nm, respectively.

Figure 3 shows FTIR spectra of $BaFe_{12-x}(GdNd)_{x/2}O_{19}$($x$ = 0–2). Peaks at 447, 530, and 591 cm^{-1} arose from the BaM structure. However, peaks at 1110, 1384, and 1631 cm^{-1} were attributed to –OH and $–COO^-$ anti-symmetric stretching.[12] The peaks that appeared from 2349 to 2923 cm^{-1} and at 3441 cm^{-1} were attributed to –CH stretching vibration and –OH stretching vibration of the hydroxyl group, respectively.[13,14]

Magnetic and Microwave Properties

Figure 4 shows results from VSM analysis of $BaFe_{12-x}(GdNd)_{x/2}O_{19}$($x$ = 0–2) calcined at 900°C.

Table II. Magnetic properties of the different samples

$BaFe_{12-x}(GdNd)_{x/2}O_{19}$	M_s (emu/g) (+0.5)	M_r (emu/g) (±0.5)	H_c (Oe) (+5)
x = 0	44.15	23.68	4930
x = 0.5	21.4	11.33	4563
x = 1	16	9.30	3568
x = 1.5	32.1	17.95	3457
x = 2	42.66	25.15	3293

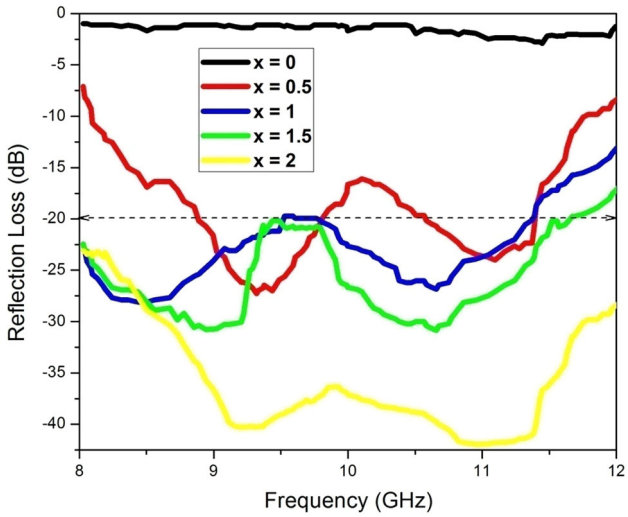

Fig. 5. Reflection loss curves for $BaFe_{12-x}(GdNd)_{x/2}O_{19}$ containing 70% ferrite and with an absorber thickness of 1.6 mm.

Magnetic data are listed in Table II. These results show that coercivity decreased with increasing substitution. The decrease in coercivity could be mainly because of the increase in particle size. Another reason could be reduction of the magneto-crystalline anisotropy field because of the change of the easy axis of magnetization from the c-axis to the basal plane. Thus, further substitution of dopants led to greater reduction of the coercivity, because of the decrease in in-plane anisotropy.[15] The maximum (44.15 emu/g) magnetization was that of the sample with x = 0; the minimum magnetization (16 emu/g) was that of the sample with x = 1. Decreasing M_s can be explained on the basis of occupation of the lattice sites by $Gd^{3+}$and Nd^{3+} ions. However, for samples with x = 0.5–1.5, owing to the different ionic radii of Gd^{3+} (0.935 Å) and Nd^{3+} (0.983 Å), from that of Fe^{3+} (0.645 Å), a decrease in super-exchange interactions between $4f_1$–$12k$ and $4f_1$–$2a$ was expected. Thus, magnetization of the samples decreased.[16]

Reflection loss can be expressed as a function of normalized input impedance for a metal backed absorber. The normalized input impedance (Z_{in}) of a microwave-absorbing layer backed by a reflector is given by:

Table III. Microwave characteristics of $BaFe_{12-x}(GdNd)_{x/2}O_{19}$ (x = 0–2)

$BaFe_{12-x}(GdNd)_{x/2}O_{19}$	Domain wall resonance (GHz)	Natural resonance (GHz)	Bandwidth (GHz) (RL > −20 dB)	Reflection loss (f_1) (dB)	Reflection loss (f_2) (dB)
x = 0	11.44	–	–	−3	–
x = 0.5	9.3	11	2.6	−27	−23.96
x = 1	8.4	10.7	3.4	−28.2	−26.8
x = 1.5	9	10.66	3.6	−30.8	−31.1
x = 2	9.24	11.1	4	−40.5	−42.1

$$Z_{\text{in}} = \frac{Z_{\text{i}}}{Z_{\text{o}}} = \left(\frac{\mu_{\text{r}}}{\varepsilon_{\text{r}}}\right)^{0.5} \tanh\left[\frac{j2\pi(\mu_{\text{r}}\varepsilon_{\text{r}})^{0.5} fd}{c}\right] \quad (3)$$

where Z_{in} is the normalized input impedance at the absorber surface, Z_{i} is the input impedance, and Z_{o} is the impedance of free space, μ_{r} and ε_{r} are relative permeability and permittivity of the medium, f, is the frequency of microwaves in free space, c is the velocity of the electromagnetic wave, and d is the thickness of absorber. Reflection loss, the ratio of reflected power to incident power, is related to Z_{in} as shown below:

$$\text{Reflection loss (dB)} = 20\log_{10}\left[\frac{(Z_{\text{in}}-1)}{(Z_{\text{in}}+1)}\right]. \quad (4)$$

Figure 5 shows the variation of reflection loss as a function of frequency in the range 8–12 GHz for x = 0–2 hexaferrite samples 1.6 mm thick and 70 mass.% ferrite. Here, the bandwidth is defined as the frequency width in which the reflection loss is more than −20 dB. The measured microwave properties are listed in Table III. From these results it is apparent that increasing x to 2 resulted in the highest value of the reflection loss (−42.1 dB) at the matching frequency of 11.1 GHz.The ferromagnetic resonance, f_r, of barium ferrite can obtained by use of Eq. 5:

$$2\pi f_{\text{r}} = \gamma\sqrt{H_\theta H_\varphi}, \quad (5)$$

where γ is the gyromagnetic ratio, H_θ is the out of plane anisotropy field, and $H_\varnothing$ is the in-plane anisotropy field. From this equation, it can be inferred that the ferromagnetic resonance frequency is closely related to the magnetocrystalline anisotropy field H_θ and to $H_\varnothing$ of the barium ferrites. Indeed, H_θ and $H_\varnothing$ are related to $Gd^{3+}$and Nd^{3+} substitution.[17] Two resonance absorption peaks have been detected for the ferrites. The resonance absorption peak at low frequency is related to domain wall resonance whereas the peak at high frequency is related to natural resonance.[15] The most striking result emerging from the data is that Gd–Nd substituted barium ferrite had a wide bandwidth (>−20 dB) and high reflection loss in the frequency band of 8–12 GHz. It was clear that the maximum bandwidth covered by this ferrite was approximately 4 GHz with reflection loss greater than −42 dB. Substitution of iron by other ions in ferrites changed the direction of the magneto-crystalline anisotropy of the material from the c-axis toward the a–b basal plane. The reason for this anisotropy could be effective coupling of the spins of the magnetic ions and crystalline electric fields affecting the ions via spin–orbit coupling.[18]

CONCLUSIONS

Gd–Nd-substituted barium hexaferrite ceramics were synthesized by use of an economical and simple co-precipitation method. We showed that Gd–Nd-substituted BaM can be a suitable absorber with a maximum RL of −42.1 dB and bandwidth of 4 GHz, with reflection loss being greater than −20 dB in the frequency range of the X-band (8–12 GHz).The samples had hexagonal structures, as confirmed by XRD studies and by calculation of cell constants and cell volume from XRD data. In comparison with pure barium hexaferrite, saturation magnetization and remanence decreased with increasing Gd–Nd concentration.

REFERENCES

1. P. Shepherd, K.K. Mallick, and R.J. Green, *J. Magn. Magn. Mater.* 311, 683 (2007).
2. S. Chang, S. Kangning, and C. Pengfei, *J. Magn. Magn. Mater.* 324, 802 (2012).
3. L. Zhao, X. Lv, Y. Wei, C. Ma, and L.N. Zhao, *J. Magn. Magn. Mater.* 332, 44 (2013).
4. S.K. Chawla, R.K. Mudsainiyan, S.S. Meena, and S.M. Yusuf, *J. Magn. Magn. Mater.* 350, 23 (2014).
5. J.A. Kohn, D.W. Eckart, and C.F. Cook Jr, *Sci.* 172, 519 (1971).
6. Z. Mosleh, P. Kameli, M. Ranjbar, and H. Salamati, *Ceram. Int.* 40, 7279 (2014).
7. M.A. Ahmed, N. Helmy, and S.I. El-Dek, *Mater. Res. Bull.* 48, 3394 (2013).
8. I. Bsoul and S.H. Mahmood, *J. Alloys Compd.* 489, 110 (2010).
9. M. Bahgat, M. Radwan, and M.M. Hessien, *J. Magn. Magn. Mater.* 310, 107 (2007).

10. F. Sánchez-De Jesús, A.M. Bolarín-Miró, C.A. Cortés-Escobedo, R. Valenzuela, and S. Ammar, *Ceram. Int.* 40, 4033 (2014).
11. M. Jamalian, A. Ghasemi, E. Paimozd, and J. Elect, *Mater.* 43, 1076 (2014).
12. W. Yongfei, L. Qiaoling, Z. Cunrui, and J. Hongxia, *J. Alloys Compd.* 467, 284 (2009).
13. X. Yang, Q. Li, J. Zhao, B. Li, and Y. Wang, *J. Alloys compd.* 457, 312 (2009).
14. M.G. Hasab, S.A. Seyyed Ebrahimi, and A. Badiei, *J. Eur. Ceram. Soc.* 27, 3637 (2007).
15. M. Jamalian, *J. Magn. Magn. Mater.* 378, 217 (2015).
16. A. Sharbati, J.M. Verdi Khani, and G.R. Amiri, *Solid State Commun.* 152, 199 (2012).
17. M. Jamalian, A. Ghasemi, and E. Paimozd, *Curr. Appl. Phys.* 14, 909 (2014).
18. M. Mozaffari, A. Arab, M.H. Yousefi, and J. Amighian, *J. Magn. Magn. Mater.* 322, 2670 (2010).